ASTRONOMY AND SPACE SCIENCE
www.csiro.au

ASKAP antenna aperture efficiency estimation

David McConnell, Keith Bannister, Aidan Hotan

ASKAP Commissioning and Early Science Memo 005
June 3, 2015

CSIRO Astronomy and Space Science
Cnr. Vimiera and Pembroke Roads
PO Box 76, Epping, NSW 1710, AUSTRALIA Telephone : +61 2 9372 4100
Fax : +61 2 9372 4310

Contents

Contents

Summary

We describe a procedure for estimating system noise and aperture efficiency for elements of a radio synthesis array. The method uses the known flux-density of a cosmic calibration source and knowledge of the variation in sky brightness to scale the visibility noise and determine the antenna sensitivity—the increment of antenna temperature for a given increment of incident power flux-density. We apply this to the six ASKAP antennas currently equipped with Mark I Phased Array Feeds (PAFs) at a frequency of 1390MHz for which we have a reliable model of the sky brightness temperature. The results are summarised in the following table.

Antenna	Antenna sensitivity		Efficiency	T_{sys}
	K (mK/Jy)	K^{-1} (Jy/K)	η	(K)
AK01	27.5	36.4	0.67	110.3
AK03	27.3	36.6	0.67	98.6
AK06	27.8	36.0	0.68	109.4
AK08	29.0	34.5	0.71	112.6
AK09	31.1	32.2	0.76	117.8
AK15	29.8	33.6	0.73	117.4

Table 0.1: Results summary of the analysis for the axial beam on all BETA antennas.

1 Introduction

[1] The cosmic signal of interest to a radio telescope falls on the receiver at its focus and produces noise at the receiver input. If the signal's spectral flux-density (expressed in watts/metre^2/Hz) is S, and it completely and uniformly illuminates the telescope's aperture of area A, then the magnitude of the receiver input can be expressed as an equivalent temperature, the "antenna temperature"[2]

$$T_A = \frac{A}{2k} S \tag{1.1}$$

where k is Boltzmann's constant. This input noise is amplified by some factor G at the receiver output.

In practice, there is additional noise at the receiver output originating from spurious input noise (eg. thermal emission from the ground through "spillover" responses) and in the receiver's elec-

[1] For the sake of brevity, this description of radio telescope sensitivity is kept simple. See (for example) Crane & Napier (1989) for a more thorough treatment.

[2] This diagram from Kraus (1966) illustrates the concept of antenna temperature and its equivalents.

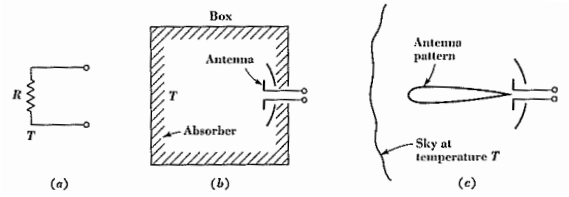

tronics. Disregarding the common gain G, the total noise at the output is the sum

$$T_{sys} = T_{rec} + T_{spill} + T_A \tag{1.2}$$

The ideal of complete aperture illumination cannot be realised, and so (1.1) should be written

$$T_A = \frac{\eta A}{2k} S = KS \tag{1.3}$$

where η is the efficiency and K is known as the antenna sensitivity and has units K Jy^{-1}.

The radiometric performance of a radio telescope is determined by two quantities: T_{sys} and η. These can be quantified by observing a cosmic source of known flux-density S_i and measuring the increment Δw in the total noise w and noting that

$$\Delta T = \frac{A_e}{2k} S_i \tag{1.4}$$

$$\Delta w \equiv \Delta T \tag{1.5}$$

so that

$$T_{sys} = \frac{w}{\Delta w} \frac{\eta A}{2k} S_i \tag{1.6}$$

$$\frac{T_{sys}}{\eta} = \frac{w}{\Delta w} \frac{A}{2k} S_i \tag{1.7}$$

This measurement cannot separately determine T_{sys} and η.

In this memorandum we describe a procedure to separately determine T_{sys} and η by using the comparatively well-known variation of radiation temperature across the sky. Specifically, we seek large sky-temperature variations by allowing the Galactic Plane to drift through the antennas' beam and observing the variations induced in receiver output noise.

2 Method

For an interferometer formed from two identical antennas, the noise in both the real and imaginary components of the visibility measured over bandwidth Δf and time period τ is given by

$$\Delta S = \frac{1}{K} \frac{T_{sys}}{\sqrt{2 \Delta f \tau}} \tag{2.1}$$

Provided the visibility from the interferometer is calibrated using an observation of a source of known flux-density, ΔS is a measureable quantity.

As is seen from (1.3), although the source flux-density may be known, T_A is unknown by a factor η. However, if we fill the antenna beam with radiation of a known temperature T_{sky}, we can equate T_A with T_{sky} and write T_{sys} as the sum of a known and an unknown component:

$$T_{sys} = T_{rec} + T_{spill} + T_{sky} \tag{2.2}$$

$$= T_1 + T_{sky} \tag{2.3}$$

then from (2.1) above we have

$$\Delta S = \frac{1}{K}\frac{(T_1 + T_{sky})}{\sqrt{2\Delta f \tau}} \tag{2.4}$$

or

$$\text{SEFD} = \frac{1}{K}(T_1 + T_{sky}) \tag{2.5}$$

where SEFD is the System Equivalent Flux-Density:

$$\text{SEFD} = \Delta S\sqrt{2\Delta f \tau} \tag{2.6}$$

We can measure SEFD for a range of T_{sky} values. We perform drift scans, holding the antenas fixed pointing at the southern meridian, allowing the Galactic Plane to drift through the beam. In this way we expect both T_{rec} and T_{spill} to remain constant. We then fit a linear relation to the data:

$$y = ax + b \tag{2.7}$$
$$y \equiv \text{SEFD} \tag{2.8}$$
$$x \equiv T_{sky} \tag{2.9}$$
$$K = \frac{1}{a} \tag{2.10}$$
$$T_1 = Kb \tag{2.11}$$

The efficiency is then

$$\eta = \frac{1}{a}\frac{2k}{A} \tag{2.12}$$

(2.13)

3 Observations

Drift scans of the Galactic Plane were done in BETA bands 1 and 3. The details are given in table 3. In both cases, the phase tracking centre was set to the South Celestial Pole so that no phase rotation or delay compensation was performed.

4 The Global Sky Model

The Global Sky Model (GSM) de Oliveira-Costa et al. (2008)[3] is an all-sky model of diffuse radio emission. It is derived by principal component analysis of publicly available radio maps with frequencies in the range 0.01–94 GHz.

To generate the all sky maps, we ran the GSM code using three principle components at 1 MHz intervals between 700–1800 MHz to generate a set of 1100 HealPix-formatted sky maps in galactic co-ordinates, calibrated in K. Using the python package, HealPy, (in our script: scan_gsm.py)

[3] http://space.mit.edu/~angelica/gsm/index.html

Band	1	3	
Frequency	711 - 1015	1224 - 1528	MHz
SBID	1139	1252	
Footprint	Line : pitch = 1.46	Square : pitch = 0.78	degrees
Beam weights	201411130423_5872_9beams	201412100135_6384_9beams	
Start	2014-11-20 03:31:05	2014-12-11 02:26:53	UTC
Duration	04h57m35s		
Az, El	180.0,84.7	180.0,84.7	degrees
Declination	$-32{:}02$	$-32{:}02$	degrees
RA	230 - 303	235 - 308	degrees
Solar position	15:42:07, $-19{:}39{:}53$	17:12:27, $-22{:}59{:}06$	J2000
Calibration	B1934-638	B1934-638	
SBID	1141	1251	
Start	2014-11-20 08:40:00	2014-12-11 00:15:25	UTC

Table 3.1: Details of the Band 1 and Band 3 observations. SBID = Scheduling Block IDentifier.

we then extracted a strip from RA and declination ranges 15.0–20.5 h and $-31.7987 \pm 4.5^\circ$ and for each frequency and saved the results in a python pickle file.

As we mention in §6, at present we mistrust our application of the GSM in this work. As an alternative, we have used the continuum image of the southern sky produced using the 21cm multibeam receiver on the Parkes telescope. This image, the "CHIPASS" image, was formed from the original HIPASS observations by Calabretta et al. (2014). Recently, its temperature scale has been revised by Alves et al. (2014). We used that revised version of the CHIPASS image to form a sky temperature model in the region of interest.

5 Analysis

5.1 Overview

The observations result in two measurement sets, one for the calibration observation of B1934-638, and the other for the drift scan. In each case the measurement set contains visibilities for 9 beams, 15 baselines, 4 polarizations (XX, XY, YX, YY) and 16416 frequency channels ($\delta f = 18.518$kHz). The sample interval is $\tau = 5$s.

The data analysis proceeds though the following steps.

1. Selection: Visibilities are selected for a single beam over a 2MHz band ($N_f = 108$ channels) at the chosen frequency in all polarizations and baselines, from both calibration and scan data.
2. Calibration:
   - a bandpass amplitude scale is established by dividing the known flux-density of B1934-638 (Reynolds 1994) by the visibility amplitudes for each baseline and parallel polarization product (XX, YY);
   - the XY and YX scales are computed as the geometric mean of the XX and YY scales;

- these scales are established for each of the N_f frequency channels selected;
- the corresponding scan data are then multiplied by the calibration scales.

3. Noise determination: The quantity ΔS of (2.1) is determined as a time series $\Delta S(t)$ over the duration of the drift scan; see §5.2 for the details.
4. SEFD is caclulated as SEFD $= \Delta S \times \sqrt{2\delta f \tau}$ for each baseline, polarization product.
5. Each of the four sets of 15 SEFD time series are decomposed into antenna specific quantities (§5.3).
6. For the chosen frequency, a model for the sky brightness temperature T_{sky} is estimated along the path of the drift scan (§5.4) and placed on the same Right Ascension grid as the SEFD series.
7. Two forms of the SEFD function are formed: $\text{SEFD}_0 = \frac{\text{SEFD}_{XX}+\text{SEFD}_{YY}}{2}$ and $\text{SEFD}_1 = \frac{\text{SEFD}_{XY}+\text{SEFD}_{YX}}{2}$; §**??** discusses why these quantities are preferred over the raw polarization products.
8. The points $(x_i, y_i) = (T_{sky_i}, \text{SEFD}_{1i})$ are fitted to a straight line model $y(x) = ax + b$.
9. The quantities of interest are then $T_1 = T_{rec} + T_{spill} = \frac{b}{a}$, $K = \frac{1}{a}$, and $\eta = \frac{1}{a}\frac{2k}{A}$.

5.2 Noise estimation

The quantity ΔS of (2.1) is determined as a time series $\Delta S(t)$ over the duration of the drift scan; for each t, ΔS is determined for both the real and the imaginary components over an "integration cell"—a $\Delta t \times \Delta f$ window centred at t and containing $N_f \times N_t$ visibility measurements; $N_t = \frac{\Delta t}{\tau}$ and τ is the visibility sample interval. $\Delta S(t)$ is determined for visibility product (15 baselines, 4 polarizations).

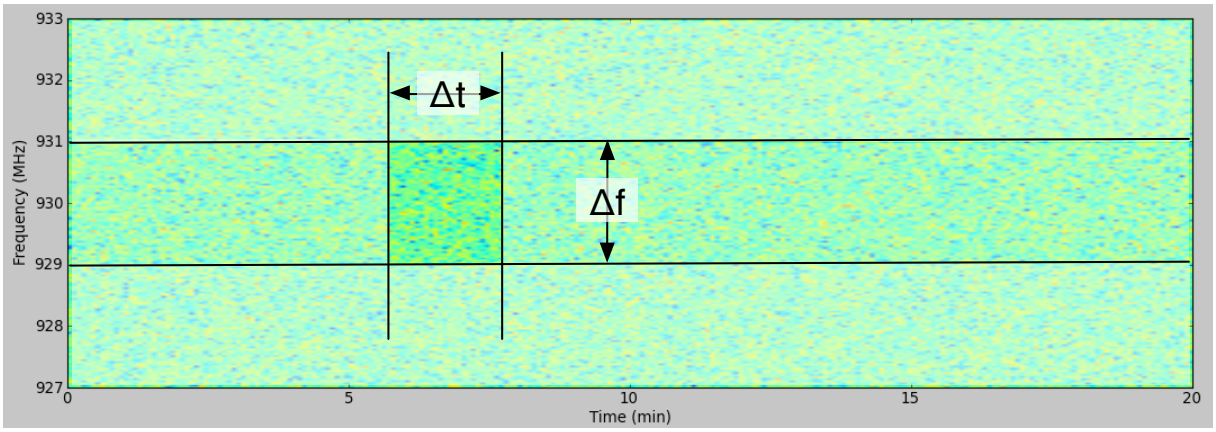

Figure 5.1: The noise amplitude is calculated in the $\Delta t \times \Delta f$ window—the "integration cell"—which slides in time to give the time series $\Delta S(t)$. This example is the real part of the XX visibility on the longest BETA baseline AK06 × AK15.

For ASKAP, the antenna sensitivity is approximately $K \sim \frac{1}{30}$K Jy^{-1}, so that most discrete sources can be neglected in the determination of T_{sys}. However, on the shorter BETA baselines, comparatively extended brightness fluctuations on the sky can produce visible fringes that invalidate the simple calculation of standard deviation over the integration cell shown in Figure 5.1. The assumption of constant mean over the cell is violated. Figure 5.2 shows an example.

The main sources of corrupting fringes are the Sun and the Galactic Plane itself, whose effective width is comparable with the fringe spacing on the shorter BETA baselines.

To estimate the true noise, we fit a simple sinusoidal model to the real (imaginary) part of the visibility over the extent of the integration cell. Althought the amplitude and frequencies of the fringe patterns change with time and frequency, within the integration cell their variation is not significant. We fit the data to a function of the form $v = p_0 \sin(p_1 t + p_2 f + p_3) + p_4 t + p_5 f$. We then use the standard deviation of the residuals as the noise estimate.

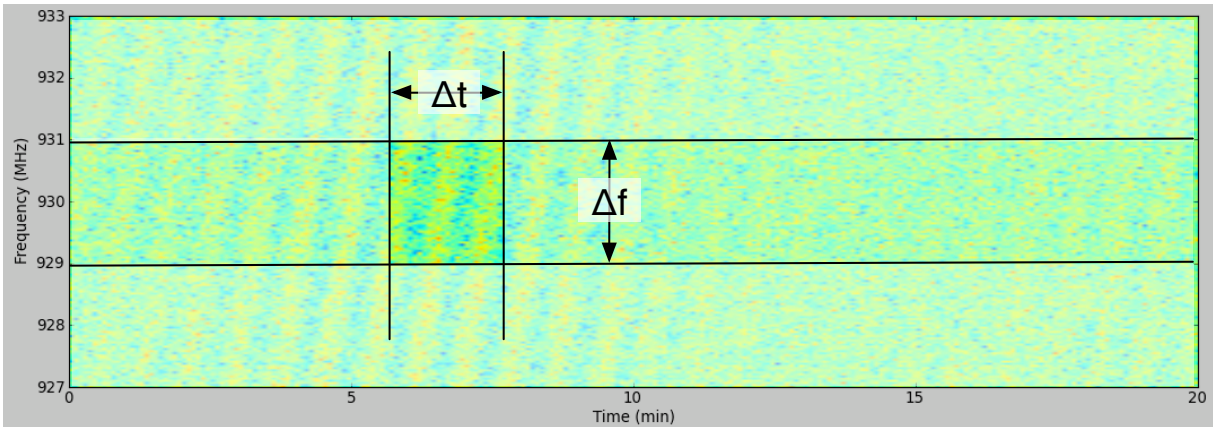

Figure 5.2: Fringes are evident in the real visibility component from the XX polarization on the short BETA baseline AK06 $\times$ AK03. At this time in the scan the Sun was close to transit.

5.3 Determining antenna-specific noise

Given the SEFD for two antennas i, j, then the noise ΔS_{ij} on the real and imaginary parts of the visibility is (Wrobel & Walker (1999), equation 9-14)

$$\Delta S_{ij} = \sqrt{\frac{\mathrm{SEFD}_i \mathrm{SEFD}_j}{2\Delta f \tau}} \tag{5.1}$$

$$\mathrm{SEFD}_{ij} = \sqrt{\mathrm{SEFD}_i \mathrm{SEFD}_j} \tag{5.2}$$

$$\log \mathrm{SEFD}_{ij} = \frac{1}{2}(\log \mathrm{SEFD}_i + \log \mathrm{SEFD}_j) \tag{5.3}$$

$$\tag{5.4}$$

so that the antenna specific quantities can be determined by inverting a set of linear equations to solve for $\mathbf{x}$ in $\mathbf{Ax} = \mathbf{B}$, where $\mathbf{B}$ is a $1 \times N_b$ matrix holding the logarithms of the SEFD_{ij}, $\mathbf{A}$ is an $N_b \times N_a$ matrix of zeroes but for $A_{ki} = A_{kj} = 1$, the k^{th} baseline being formed from antennas i and j.

5.4 Modelling the sky brightness temperature

The sky temperature models used are image cubes (axes frequency, RA, declination). To form a valid comparison to the SEFD series from the drift scan, we convolve the relevant frequency plane with an estimate of the BETA antenna primary beam power pattern. We use two methods to estimate the beams:

1. Analytically—assuming an Airy function that would result from a fully-illuminated unblocked aperture.
2. Using a holographic measurement of the beam shape. For this initial work we have only a Band 1 (711 - 1015MHz) measurement for AK06, which we use for all antennas.

Comparison of the results using the two kinds of bea estimate showed negligible difference. For the results reported here we used the analytic beam model.

For the drift scan at declination δ we compute the model sky temperature for Right Ascension α_i as

$$T_{sky}(\alpha_i) = \frac{\sum_m \sum_l T(\alpha_i + \frac{l}{\cos\delta}, \delta + m) B(l,m)}{\sum_m \sum_l B(l,m)} \tag{5.5}$$

6 Results

We present here the results of analysing the drift scan conducted in Band 3: 1224 - 1528 MHz. The data were analysed for the 2-MHz band at 1390 MHz, the centre of the CHIPASS band. Here we report results from the axial, or bore-sight beam. Analysis of the Band 1 scan produced results showing a frequency dependence that suggests some error in our application of the GSM of de Oliveira-Costa et al. (2008). Therefore we defer reports of performance in Band 1 until we have more confidence sky temperature model in that frequency range (700–1000 MHz).

Figure 6.1 summarises the analysis results for antenna AK15. Note that we observed an apparently linear change in the baseline with time (or Right Ascension). We do not know the origin of this drift, which was observed to soem extent on all antennas, but have used an additional term in the fit. No such drift was observed in the Band 1 data.

Table 6 shows the fitted parameters for all BETA antennas.

	AK06	AK01	AK03	AK15	AK08	AK09
K^{-1} (Jy/K)	36.0	36.4	36.6	33.6	34.5	32.2
SEFD (no sky) (Jy)	3936	4014	3612	3940	3886	3794
Drift rate (Jy/ s^{-1})	-0.124	-0.117	-0.085	-0.090	-0.098	-0.093
η	0.68	0.67	0.67	0.73	0.71	0.76
$T_{rec} + T_{spill}$ (K)	109.4	110.3	98.6	117.4	112.6	117.8

Table 6.1: Results of the analysis for al BETA antennas. The first two rows are the fitted parameters a and b/a from equation 2.7; the third row gives the values of the parameter introduced to cope with the linear drift; the final two rows give the derived parameters (2.12, 2.11)

6.1 Sources of systematic error

We briefly consider factors that may bias the results as presented above.

Sky model For this analysis, the sky temperature model was based on the Parkes 1.4GHz continuum image produced by Calabretta et al. (2014). The temperature scale presented in that work was based on a "full beam" calibration. Since then, Alves et al. (2014) have converted the image to the more useful main beam scale: they adopt a scale of $T_b/S = 0.70 \pm 0.07$K/(Jy beam^{-1}) The 10% uncertainty in T_{sky} in equation 2.5 will propagate to a 10% uncertainty in η and $T_1 = T_{rec} + T_{spill}$.

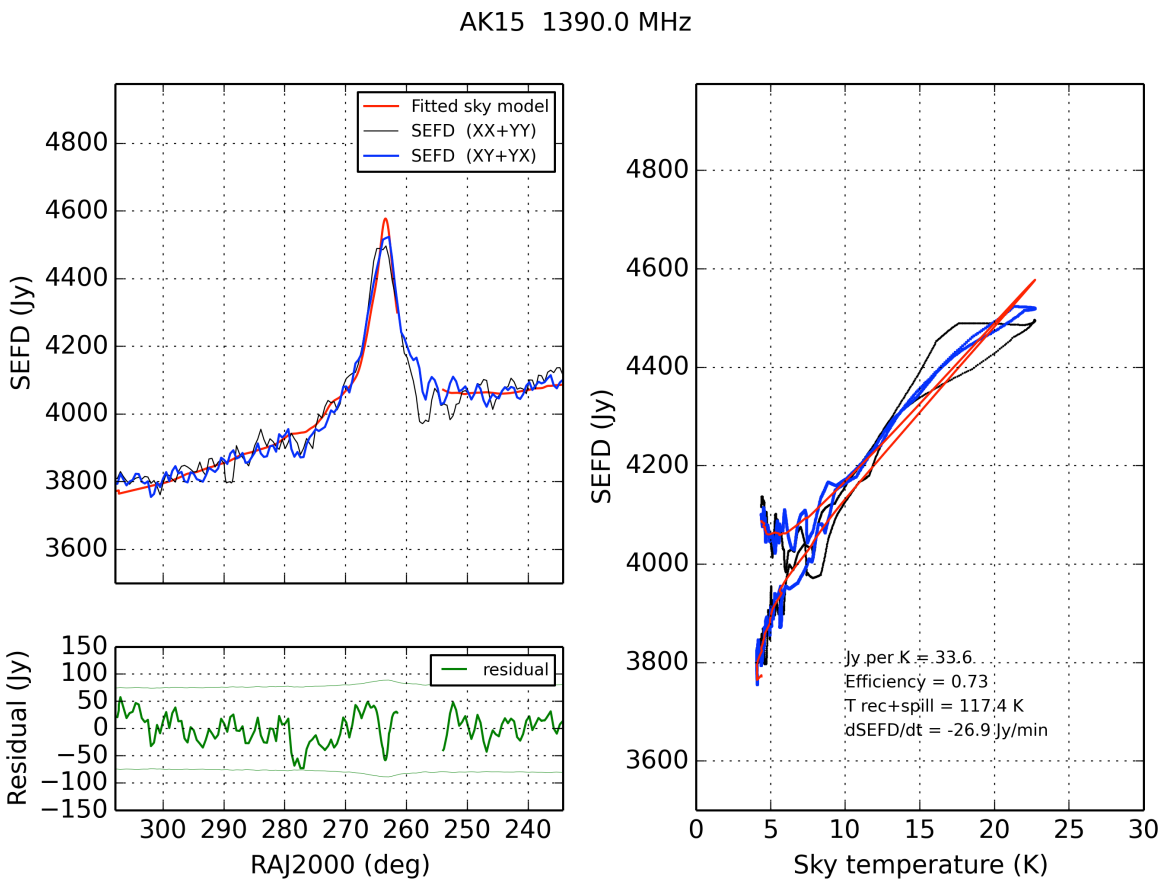

Figure 6.1: Analysis of the drift scan for antenna AK15. The upper-left panel show SEFD as a function of RA in both polarization combinations described in §**??**. The fitted model (sky temperature plus linear drift with time) is shown in red; the fit is to the XY+YX (blue) data. The lower-left panel shows the residuals; the faint upper and lower line shows the expected 2σ level, determined from the number of samples in each integration cell. The right panel shows data and fit on the temperature−SEFD plane, with the same line-styles as the upper- left plot.

Declination pointing error Mechanical pointing errors of the antennas would shift the response to a different track across the sky than has been assumed. Declination gradients in the sky temperature would then introduce a systematic error. From the declination gradient in the sky model, we estimate the error in η to be of the order of 0.02 per degree of pointing error. Pointing errors have been measured and are at most 3 minutes of arc, so this source of error in η is neglible.

Beam size assumption Because the sky model is convolved with an assumed primary beam (see §5.4), a false assumption of beam size will propagate to an error in η. The effect should be greatest for parts of the sky where the brightness temperature changes on scales smaller than the beam. We have estimated, by varying the assumed beam size, that for these data a 10% error in assumed beam size leads to less than 1% error in η. Note that in other work we have shown the beam-size variation amongst antennas to be much less than this wide 10% trial variation.

7 Discussion and future work

In the future we will:

- attempt to gain confidence in a sky temperature model over the entire ASKAP tuning range;
- investigate the source of the linear drift observed at 1390 MHz;
- explore the variation of $T_{rec} + T_{spill}$ with elevation to help understand the distinction between the two quantities;
- measure the variation of both η and $T_{rec} + T_{spill}$ for beams offset from the boresight;
- investigate the dependence on η and $T_{rec} + T_{spill}$ on the algorithm used for computing beam weights.

8 Symbols

A	Area of antenna	m^2
k	Boltzmann's constant	$m^2 kg\ s^{-2} K^{-1}$
K	Antenna sensitivity	$K\ Jy^{-1}$
S	Power spectral flux-density	$W\ m^{-2}\ Hz^{-1}$
T	Temperature	K
T_A	Antenna temperature	K
T_{rec}	Receiver temperature	K
T_{spill}	Equivalent temperature of spillover noise	K
T_{sys}	Equivalent temperature of total system noise	K
η	Aperture efficiency	
Δf	Bandwidth of noise determination cell	Hz
Δt	Duration of noise determination cell	s
δf	Channel bandwidth	Hz
τ	Sample interval (Correlator integration time)	s

References

Alves, M. I. R., Calabretta, M., Davies, R. D., Dickinson, C., Staveley-Smith, L., Davis, R. J., Chen, T., & Barr, A. 2014, ArXiv e-prints

Calabretta, M. R., Staveley-Smith, L., & Barnes, D. G. 2014, PASA, 31, 7

Crane, P. C. & Napier, P. J. 1989, in Astronomical Society of the Pacific Conference Series, Vol. 6, Synthesis Imaging in Radio Astronomy, ed. R. A. Perley, F. R. Schwab, & A. H. Bridle, 139

de Oliveira-Costa, A., Tegmark, M., Gaensler, B. M., Jonas, J., Landecker, T. L., & Reich, P. 2008, MNRAS, 388, 247

Kraus, J. D. 1966, Radio Astronomy (Cygnus-Quasar Books)

Reynolds, J. E. 1994, A Revised Flux Scale for the AT Compact Array, Tech. Rep. AT/39.3/040, ATNF, CSIRO

Wrobel, J. M. & Walker, R. C. 1999, in Astronomical Society of the Pacific Conference Series,

Vol. 180, Synthesis Imaging in Radio Astronomy II, ed. G. B. Taylor, C. L. Carilli, & R. A. Perley, 171

CONTACT US

t 1300 363 400
+61 3 9545 2176
e enquiries@csiro.au
w www.csiro.au

YOUR CSIRO

Australia is founding its future on science and innovation. Its national science agency, CSIRO, is a powerhouse of ideas, technologies and skills for building prosperity, growth, health and sustainability. It serves governments, industries, business and communities across the nation.

FOR FURTHER INFORMATION

CSIRO Astronomy and Space Science
David McConnell
t +61 2 9372 4132
e David.McConnell@csiro.au
w Astronomy and Space Science

CSIRO Astronomy and Space Science
Aidan Hotan
t +61 2 9372 4425
e Aidan.Hotan@csiro.au
w Astronomy and Space Science